JACS
JOURNAL OF THE AMERICAN CHEMICAL SOCIETY
Article
pubs.acs.org/JACS

Chasing the Evasive Fe=O Stretch and the Spin State of the Iron(IV)–Oxo Complexes by Photodissociation Spectroscopy

Erik Andris,[†] Rafael Navrátil,[†] Juraj Jašík,[†] Thibault Terencio,[†] Martin Srnec,*[,§] Miquel Costas,*[,‡] and Jana Roithová*[,†]

[†]Department of Organic Chemistry, Faculty of Science, Charles University, Hlavova 2030/8, 12843 Prague 2, Czech Republic
[‡]Departament de Quimica and Institute of Computational Chemistry and Catalysis (IQCC), University of Girona, Campus Montilivi, Girona 17071, Spain
[§]J. Heyrovsky Institute of Physical Chemistry of the CAS, v.v i., Dolejškova 2155/3, 182 23 Prague 8, Czech Republic

Supporting Information

ABSTRACT: We demonstrate the application of infrared photodissocation spectroscopy for determination of the Fe=O stretching frequencies of high-valent iron(IV)–oxo complexes $[(L)Fe(O)(X)]^{2+/+}$ (L = TMC, N4Py, PyTACN, and X = CH_3CN, CF_3SO_3, ClO_4, CF_3COO, NO_3, N_3). We show that the values determined by resonance Raman spectroscopy in acetonitrile solutions are on average 9 cm^{-1} red-shifted with respect to unbiased gas-phase values. Furthermore, we show the assignment of the spin state of the complexes based on the vibrational modes of a coordinated anion and compare reactivities of various iron(IV)–oxo complexes generated as dications or monocations (bearing an anionic ligand). The coordinated anions can drastically affect the reactivity of the complex and should be taken into account when comparing reactivities of complexes bearing different ligands. Comparison of reactivities of $[(PyTACN)Fe(O)(X)]^+$ generated in different spin states and bearing different anionic ligands X revealed that the nature of anion influences the reactivity more than the spin state. The triflate and perchlorate ligands tend to stabilize the quintet state of $[(PyTACN)Fe(O)(X)]^+$, whereas trifluoroacetate and nitrate stabilize the triplet state of the complex.

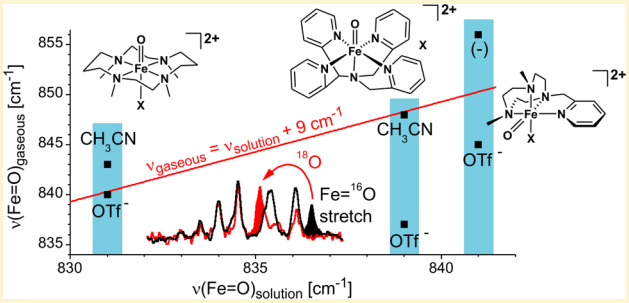

INTRODUCTION

Non-heme high-valent iron–oxo chemistry is a rapidly evolving field with interdisciplinary connections between organic, inorganic, and theoretical chemistry. The importance of non-heme iron–oxo compounds in many enzymatic reactions[1] has been appreciated mainly after the seminal works of Bollinger and Krebs.[2] The first X-ray structure characterization of a non-heme iron(IV)–oxo complex from the laboratories of Nam and Que enabled development of synthetic models that to a great extent facilitated our understanding of these reactive species and their function.[3−5] Characterization of the active iron centers currently relies mainly on UV/vis, Mössbauer, resonance Raman (rR), electron paramagnetic resonance, and X-ray spectroscopic techniques. As first demonstrated by Que and Nam,[6] resonance Raman spectroscopy usually provides the most direct evidence for the Fe=O moiety.[5a,7,8] The rR method takes advantage of resonance enhancement and thus relies on the presence of intense electronic absorption features. These are, however, not always present.[9,10] In addition, the aforementioned methods have limitations when dealing with complex mixtures. As a result, minor—though important—species may stay unnoticed. As numerously reported, mass spectrometry (MS) is an ideal tool for detection of reactive species present in low concentrations (dynamic range of a standard mass spectrometer is ~10^4–10^6).[11−13] The requirement of detailed structural information on the detected ions urged the development of novel techniques that combine MS with other spectroscopic methods such as infrared (IR) spectroscopy.[14]

Our approach, helium tagging infrared photodissociation spectroscopy (IRPD), consists of trapping the ions of interest in a cryogenic ion trap (~3 K) filled with helium. The ions are collisionally cooled and form weakly bound complexes with helium atoms. The complexes, irradiated by a tunable IR beam, detach helium if they absorb a photon. Hence, we obtain IR spectra as a dependence of the depletion of the helium complexes on the IR wavenumber.[15]

Herein, we report a set of IRPD spectra of representative non-heme iron(IV)–oxo complexes with a special emphasis on the Fe=O stretching vibration. The interface of electrospray ionization (ESI) serves to transfer the complexes from their acetonitrile solution to the gas phase. Assignment of vibrational bands to the Fe=O stretching modes is based on the ^{18}O labeling, which has been done by the oxygen atom exchange with $H_2{}^{18}O$ (Chart 1).[16]

Received: November 29, 2016
Published: January 26, 2017

DOI: 10.1021/jacs.6b12291
J. Am. Chem. Soc. 2017, 139, 2757–2765

Chart 1. Investigated Complexes and Their Fe=O Stretching Frequencies[a]

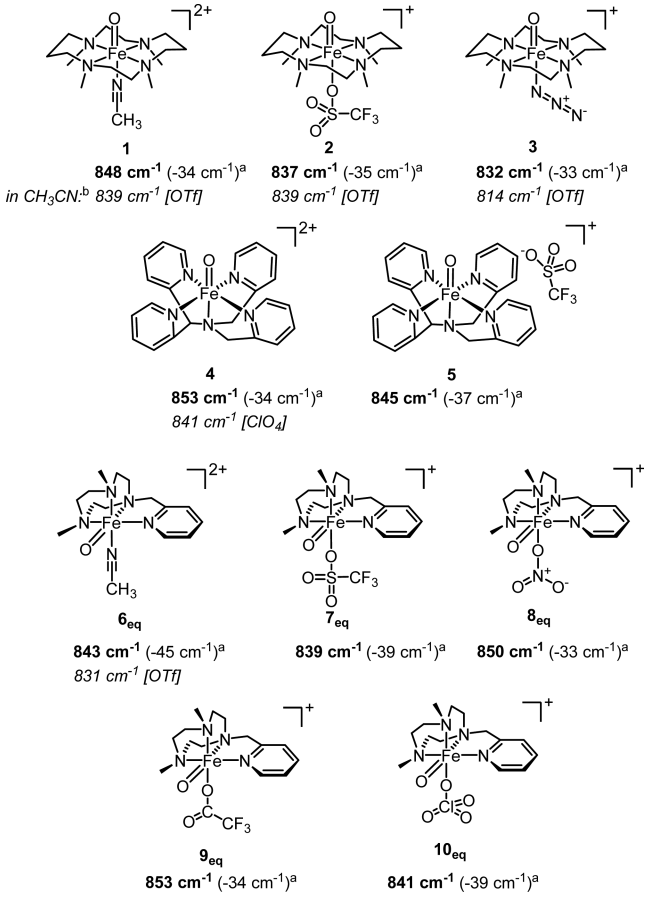

[a]Spectral shift upon ^{18}O labeling. [b]Frequencies of the complexes measured in acetonitrile solution by rR spectroscopy taken from ref 7a are given in italics. Present counterions are given in brackets.

EXPERIMENTAL AND COMPUTATIONAL DETAILS

Ion–Molecule Reactivity Studies. Experiments were performed with a triple quadrupole mass spectrometer TSQ 7000.[17] Complexes **1**, **2**, and **4**–**7** (Chart 1) were prepared according to the corresponding literature procedures[3,18,19] by oxidation of the corresponding iron(II) triflate precursors dissolved in acetonitrile (typically 0.1–1 mM) by either iodosobenzene (**1**, **2**, **4**, or **5**) or peracetic acid (**6** or **7**). Complex **3** was generated from the solution containing **1** by addition of 1 equiv of NaN_3.[20] Complexes **8**–**10** were prepared by addition of 2, 0.3, and 2 equiv of the corresponding acid to the solution containing **6**. The complexes were transferred to the gas phase by an ESI ion source at mild ionization conditions (low voltage differences during the transfer and temperature of ~60 °C). Alternatively, complexes **7**–**10** were generated by the NO_2 elimination from their $[(PyTACN)Fe(NO_3)(X)]^+$ precursors during the electrospray ionization. The NO_2 elimination requires harder ionization conditions (larger voltage differences between the transfer capillary and lenses).

Generated iron–oxo complexes were mass-selected by the first quadrupole and guided through an octopole collision cell filled with a gaseous reagent at 313 K and <0.3 mTorr pressure.[17] The nominal collision energy was set to 0 eV (Figure S1). The parent and product ions were mass-analyzed by the second quadrupole. Reaction rates were extracted from the pressure dependence of the relative abundance of the products on the reactant gas pressure.[21] Further details regarding generation of the ions and their reactivity are in the Supporting Information.

IRPD Spectra. The IRPD spectra were acquired with the ISORI instrument.[22] The ions were prepared in the same way as mentioned above, mass-selected by the first quadrupole and transferred via an octopole to a cryo-cooled wire quadrupole ion trap operated at 3 K and 1 Hz. The ions were trapped with pulsed helium buffer gas (for the time sequence of the experiment, see Figure S2 in the Supporting Information). About 1–10% of the trapped ions were transformed to the He-tagged complexes. After a time delay, the ion cloud was irradiated by eight photon pulses generated in an optical parametric oscillator/amplifier (OPO) operating at 10 Hz frequency. At 990 ms, the exit electrode of the trap was opened, the helium-tagged ions were mass-analyzed by the second quadrupole, and their number (N) was determined by the Daly-type detector operated in the ion-counting mode. In the following cycle, the light from the OPO was blocked by a mechanical shutter, giving the number of unirradiated ions (N_0). The IRPD spectra are constructed as the wavenumber dependence of $(1 - N/N_0)$. Wavenumber calibration was done using the absorption of methane and water (Figure S3), and our accuracy is ±3 cm^{-1} (precision is ±1 cm^{-1}). In the cases of **5**, **7**, and **8**, the wavelength meter WS-600 from HighFinesse GmbH was used for accurate determination of wavelength.

Density Functional Theory Calculations. Geometry optimizations and frequency calculations were performed using different density functional theory (DFT) methods as implemented in Gaussian 09:[23] B3LYP,[24] BP86,[25] B971,[26] B972,[27] B97D3,[28] BVWN5,[25a,29] OPBE,[30,31] M06,[32] M06-L,[33] M06-2X,[32] OLYP,[24b,c,30] CAM-B3LYP,[34] mPW1PW91,[35] PBE,[31] PBE0,[36] TPSS,[37] and TPSSh.[37,38] Whenever the Grimme's dispersion correction[39] is applied, it is indicated in the given figure caption (Figures S15 and S16). The basis set was constructed as a combination of 6-311+G** for C, H, O, Fe, F, and N atoms (6-311++G** for **1**, **6**, and **8**) and pc-3[40,41] for S (in **5** and **7**) and Cl atom (in **10**) and also for the carbon atom in the CF_3 group of **7** and **9**. The combined basis set is abbreviated as BS1. All optimized structures are minima on the potential energy surface confirmed by diagonalization of the mass-weighted Hessian matrix. The B3LYP-D3 calculated IR frequencies were scaled by a factor 0.99 (scaling for other methods is indicated in the corresponding figures). We have performed the calculations for all isomers (i.e., oxo in axial or equatorial position, $S = 1$ and $S = 2$) and screened the conformations of the ligands. The reported results concern the most stable structure of each isomer. All calculated Fe=O stretching frequencies are listed in Table S2.

CASSCF/CASPT2 Calculations. The complete active space self-consistent field (CASSCF)[42] and complete active space second-order perturbation theory (CASPT2)[43] calculations were carried out using the MOLCAS 8.0 program.[44] For all of the atoms, the ANO-RCC basis set, contracted to [6s5p3d2f1g] for Fe, [4s3p2d] for the ligating O and N atoms, [3s2p] for other N, O, F, and C atoms, [4s3p] for Cl and S atoms, and [2s] for H, was used. The second-order Douglas–Kroll–Hess (DKH2) one-electron spinless Hamiltonian was applied for all of the calculations in order to allow for spin-free relativistic effects.[45]

The CASSCF energies were calculated for the B3LYP-D3 optimized geometries with the 12-electrons-in-9-orbitals active space including $5 \times 3d_{Fe}$, $3 \times 2p_{oxo}$, and 1σ chelate-based orbital (Figure S25). To improve the accuracy of the calculations, the CASPT2 energies were used on the diagonal of the two-component Hamiltonian matrix. To approximate the two-electron integrals, the Cholesky decomposition technique with a threshold of 10^{-6} au was used.[46]

In all of the CASSCF calculations, a level shift of 5 au was used in order to improve convergence. In the CASPT2 calculations, none of the orbitals was frozen, and an imaginary level shift of $i0.2$ au was used to eliminate intruder states.[47]

RESULTS AND DISCUSSION

IRPD Spectroscopy. A representative IRPD spectrum of $[(TMC)Fe(O)(CH_3CN)]^{2+}$ ion (**1**, TMC = 1,4,8,11-tetramethyl-1,4,8,11-tetraazacyclotetradecane) is shown in Figure 1. The Fe=O vibration is at 848 cm^{-1} and shifts to 814 cm^{-1} upon ^{18}O labeling (Figure 1b). The theoretical IR spectrum calculated with the B3LYP-D3/6-311++G** method (Figure 1c) provides an excellent prediction of the vibrational fingerprint of the ligand, but the Fe=O stretching frequency is shifted by 66 cm^{-1} to

DOI: 10.1021/jacs.6b12291
J. Am. Chem. Soc. 2017, 139, 2757–2765

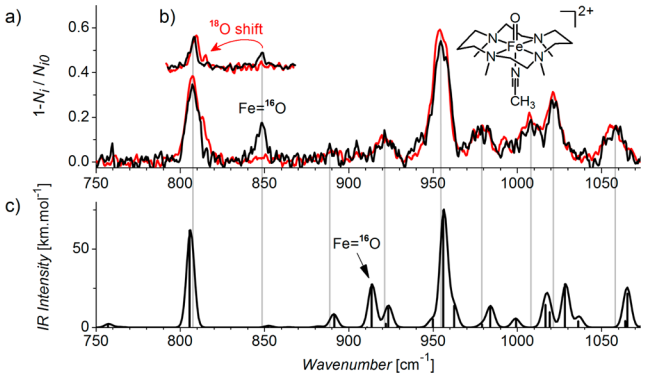

Figure 1. (a) Helium tagging IRPD spectrum of the $[(TMC)Fe(O)(CH_3CN)]^{2+}$ (**1**). (b) Spectral range with Fe=^{16}O and Fe=^{18}O stretching vibrations measured with a higher resolution. (c) B3LYP-D3/6-311++G** theoretical IR spectrum of $[(TMC)Fe(O)(CH_3CN)]^{2+}$ (scaling factor is 0.99).

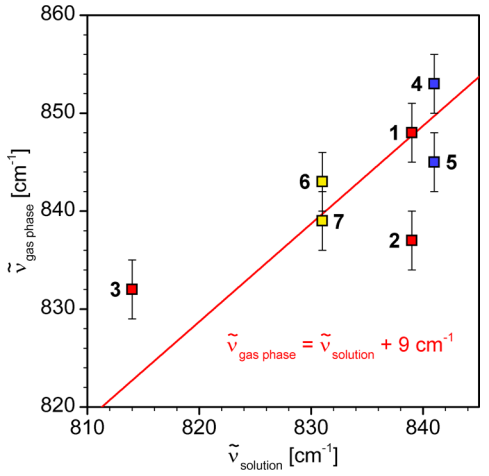

Figure 2. Comparison of the spectral shift of the Fe=O stretching vibration of the studied complexes measured in the gas phase and in acetonitrile solution (complexes with the same ligand are color-coded: TMC, red; N4Py, blue; PyTACN, yellow). The error bars refer to the calibration accuracy of ±3 cm^{-1}.

higher wavenumbers (we note in passing that we had also considered the *syn* isomer[48] (Figure S4) and ruled out its presence based on a mismatch of the IR spectra). Very similar results were obtained also for the rest of the complexes in Chart 1 (the spectra and the experimental conditions for all measurements can be found in the Supporting Information, Figures S4–S11, S13, and S14).

The determined Fe=O stretching vibrations are unique characteristics of the depicted ionic complexes. The values obtained by rR spectroscopy in solution (in italics in Chart 1) are determined with variable red shifts. It reflects the effect of the solvent as well as the effect of the counterion. For the studied dications **1**, **4** ($[(N4Py)Fe(O)]^{2+}$, N4Py = *N*,*N*-bis(2-pyridylmethyl)bis(2-pyridyl)methylamine), and **6** ($[(PyTACN)Fe(O)(CH_3CN)]^{2+}$, PyTACN = (1-[2′-(pyridyl)-methyl]-4,7-dimethyl-1,4,7-triazacyclononane)), the solution spectral shifts of −9 cm^{-1} (for **1**) and −12 cm^{-1} (for **4** and **6**) with respect to the gas phase are observed. Interestingly, singly charged complex **3** is affected even more (−18 cm^{-1}).

The big advantage of our method is that we can unequivocally characterize all species formed in solution by the speciation of the parent compound one by one (we transfer them to the gas phase and study them after mass selection). Hence, oxidation of $[(PyTACN)Fe(OTf)_2]$ in acetonitrile yields not only the $[(PyTACN)Fe(O)(CH_3CN)]^{2+}$ dication (**6**) but also the singly charged $[(PyTACN)Fe(O)(OTf)]^{+}$ (**7**) bearing the triflate ion as a ligand. We have also characterized complexes with nitrate, trifluoroacetate, and perchlorate (**8**, **9**, and **10**). Gaseous dication **6** has the Fe=O stretching vibration at 843 cm^{-1}. Coordination of nitrate and trifluoroacetate (i.e., formation of **8** and **9**) induces a blue shift of the Fe=O stretch by 7 cm^{-1} and 10 cm^{-1} with respect to **6**, whereas the other anions bring about a minor red shift (Chart 1 and Figures S10, S11, S13, and S14).

We have correlated the available Fe=O stretching vibrations determined in solution with the values determined in the gas phase for all species theoretically present in solution (mono- as well as dications). The gas-phase values are on average 9 cm^{-1} blue-shifted (Figure 2). The shift is slightly larger (11 cm^{-1}) if we assume that the solutions contain only dications. Coordination of triflate to the iron center results in a red shift of the Fe=O stretching vibration (cf. **6** vs **7** and **1** vs **2** in Figure 2). Interestingly, the Fe=O stretch is significantly red-shifted even in complex **5** (with respect to **4**) that bears triflate as a noncoordinated counterion, as evidenced from its IRPD spectrum (Figure S8). The IRPD spectrum of **5** contains S=O stretching bands that clearly correspond to a noncoordinated triflate ion. On the contrary, **2** and **7** bear triflates as ligands. This is again evidenced by the triflate bands in the IRPD spectra of the complexes (Figures S5 and S13 in the Supporting Information).

The $[(PyTACN)Fe(O)(X)]^{+}$ (X = OTf, CF_3COO, NO_3, ClO_4) complexes can exist in two isomeric forms—with the oxo group either in the equatorial or in the axial position (parallel or perpendicular to the pyridine ring plane). In addition, the complexes can be formed in the triplet (*S* = 1) or in the quintet (*S* = 2) state. According to the CASPT2 (Table 1), the isomers with

Table 1. CASPT2 Relative Energies[a] of Different Spin Isomers of $[(PyTACN)Fe(O)(X)]^{+}$ Complexes

			E^{tot}_{rel} [kcal mol^{-1}] (E^{0K}_{rel} [kcal mol^{-1}])	
notation[b]	X	spin	energy CASPT2[a]	energy B3LYP
^{3}**7**$_{eq}$	CF_3SO_3	*S* = 1	0.0 (1.1)	0.0 (0.0)
^{3}**7**$_{ax}$	CF_3SO_3	*S* = 1	2.3 (3.6)	3.3 (3.1)
^{5}**7**$_{eq}$	CF_3SO_3	*S* = 2	0.1 (0.0)	2.0 (3.2)
^{5}**7**$_{ax}$	CF_3SO_3	*S* = 2	1.5 (1.4)	3.0 (4.3)
^{3}**8**$_{eq}$	NO_3	*S* = 1	0.0 (0.0)	0.0 (0.0)
^{3}**8**$_{ax}$	NO_3	*S* = 1	2.6 (2.4)	2.6 (2.8)
^{5}**8**$_{eq}$	NO_3	*S* = 2	2.1 (1.5)	3.0 (3.6)
^{5}**8**$_{ax}$	NO_3	*S* = 2	0.4 (0.0)	0.7 (1.1)
^{3}**9**$_{eq}$	CF_3COO	*S* = 1	0.0 (0.0)	0.0 (0.0)
^{3}**9**$_{ax}$	CF_3COO	*S* = 1	5.2 (5.0)	4.7 (4.5)
^{5}**9**$_{eq}$	CF_3COO	*S* = 2	3.0 (2.5)	3.9 (3.4)
^{5}**9**$_{ax}$	CF_3COO	*S* = 2	3.5 (2.8)	4.0 (3.3)
^{3}**10**$_{eq}$	ClO_4	*S* = 1	1.0 (2.6)	0.0 (0.0)
^{3}**10**$_{ax}$	ClO_4	*S* = 1	3.2 (4.9)	3.3 (3.2)
^{5}**10**$_{eq}$	ClO_4	*S* = 2	0.0 (0.0)	1.6 (3.2)
^{5}**10**$_{ax}$	ClO_4	*S* = 2	3.7 (4.7)	2.1 (2.7)

[a]Calculations were performed with CASPT2(12,9)/ANO-RCC at geometries optimized at the B3LYP-D3 level of theory as described in the experimental details. The numbers in brackets are the CASPT2 energies corrected by zero-point vibrational energy calculated at the B3LYP-D3 level. [b]The index refers to the $[(PyTACN)Fe(O)(X)]^{+}$ isomer with the oxo group in the equatorial (eq) or axial (ax) position.

DOI: 10.1021/jacs.6b12291
J. Am. Chem. Soc. 2017, 139, 2757–2765

the oxo in the equatorial position are favored for all complexes. The nitrate and trifluoroacetate ligands stabilize the S = 1 spin states. For the complex with the triflate ligand, both spin states are almost isoenergetic, with the high-spin-state isomer $^5\mathbf{7}_{eq}$ being slightly preferred over $^3\mathbf{7}_{eq}$. The perchlorate ligand favors the S = 2 spin state. The CASPT2 energies agree relatively well with the predictions obtained by DFT using the B3LYP functional for **8** and **9** but not for **7** and **10** (Table 1). We have tested several other DFT functionals. Most of them render relative energies of the spin isomers completely wrong.[49] The B3LYP functional also outperforms the other functionals in the predictions of IR spectra.[50] A notable exception is that pure DFT functionals (e.g., M06L) give a better estimate of the Fe=O frequency (but a worse description of the ligand skeletal vibrations; see Figures S15 and S16).[51]

To further substantiate the power of our approach, we have attempted to prepare axial isomers of $[(PyTACN)Fe(O)(X)]^+$ by the gas-phase elimination of the $NO_2^\bullet$ radical from the $[(PyTACN)Fe(NO_3)(X)]^+$ precursors.[52] We have recently shown that this "nitrate cleavage method" for $[(PyTACN)Fe(NO_3)_2]^+$ leads dominantly to the generation of the quintet state of the $[(PyTACN)Fe(O)(NO_3)]^+$ isomer with the oxo in the axial position ($^5\mathbf{8}_{ax}$).[49] Hence, next to the S = 1 isomer $^3\mathbf{8}_{eq}$ obtained classically from solution, we have an independent access to the S = 2 isomer $^5\mathbf{8}_{ax}$. We set out to determine the difference in the Fe=O vibration frequency between these spin isomers.

Comparison of the IRPD spectrum of $^3\mathbf{8}_{eq}$ and its ^{18}O-labeled analogue led to a clear assignment of the Fe=O band at 850 cm^{-1} (cf. Figure S10). Figure 3a shows the comparison of the spectra in the lower wavenumber range obtained for $^3\mathbf{8}_{eq}$ and $^5\mathbf{8}_{ax}$. The spectra were obtained as a difference between the spectra of ions generated from solution and by the nitrate cleavage (see Figure S10 in the Supporting Information). The Fe=O stretch of $^5\mathbf{8}_{ax}$ lies at 851.5 cm^{-1}. The difference between $^3\mathbf{8}_{eq}$ and $^5\mathbf{8}_{ax}$ is thus just 1 cm^{-1} (see the red and blue spectra in Figure 3a). While

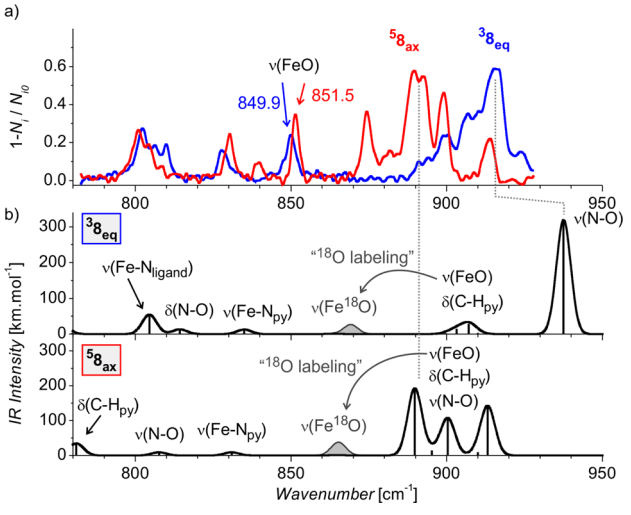

Figure 3. (a) IRPD difference spectra (cf. Figure S10) of the $[(PyTACN)Fe(O)(NO_3)]^+$ isomers generated by ligand exchange from the solution of $[(PyTACN)Fe(O)(CH_3CN)]^{2+}$ (blue trace) and generated in the gas phase from $[(PyTACN)Fe(NO_3)_2]^+$ by the nitrate cleavage (red trace). (b) Theoretically predicted spectra of $^3\mathbf{8}_{eq}$ and $^5\mathbf{8}_{ax}$ at the B3LYP-D3/6-311++G** level of theory scaled by 0.99. The predictions of the red shift of the Fe=O vibration upon ^{8}O labeling are shown in gray.

the Fe=O stretching vibration is almost unaffected by the spin state, the N−O vibrations of the nitrate ligand differ substantially (see the bands above 870 cm^{-1} in Figure 3a).[49] The agreement with the theoretical IR spectra is not great, but we show it in order to demonstrate that the large difference between the N−O stretches is expected, as well as the minor difference between the Fe=O stretches (as usually blue-shifted by almost 60 cm^{-1} in the theoretical spectra).

The nitrate cleavage approach to preparation of $[(PyTACN)Fe(O)(CF_3COO)]^+$ provides—similarly as above—ions with the IRPD spectrum distinctly different from that of the analogous ions generated from solution (cf. the red and the black spectrum in Figure 4a).

Detailed inspection shows that the spectrum of ions transferred from the solution of iron(IV) complex is composed of two components (upper trace). In addition to the bands present in the spectrum of the gas-phase-generated ions (middle trace), there are also several unique bands. We have subtracted the spectrum of the gas-phase-generated ions and obtained the IR spectrum of the second component (lower trace; for details of the spectra separation, see the Supporting Information Figure S12). The major difference is located in the range of 1130−1180 cm^{-1}. The B3LYP analysis shows that the observed bands correspond to the C−F vibrations. These vibrations are influenced by the spin state of the complex. In theory, the lowest-energy C−F vibrational band of the S = 1 complexes is red-shifted with respect to the corresponding band of the S = 2 complexes. Opposite, but less pronounced, shifts can be observed for the C=O vibration and the other C−F vibrations (cf. Figure 4b). Analogous differences stand out if we compare the red and blue spectrum in Figure 4a.

As a result, we assign the red spectrum (ions generated by the nitrate cleavage) to the S = 2 complexes (the lowest-lying C−F vibration band is blue-shifted, whereas the C=O vibration is red-shifted with respect to the bands in the blue spectrum). The blue spectrum accordingly corresponds to the S = 1 complexes. Electrospray ionization of the complexes oxidized in solution thus leads to a mixture of the spin isomers (black spectrum).

The separation process provides an estimate that about 30% of the complexes transferred from the solution should be in the quintet state (see Figure S12). The probable reasoning is that the solution dominantly contains dication $^3\mathbf{6}$ that coordinates CF_3COO^- during the electrospray process. If trifluoroacetate coordinates to the equatorial position, it leads to $^5\mathbf{9}_{ax}$—the more stable spin isomer with the oxo in the axial position. Alternatively, the coordination of the anion to the axial position leads to the formation of $^3\mathbf{9}_{eq}$. This line of reasoning also explains why nitrate-coordinated complexes **8** are obtained from the oxidized solution in a similar ratio of $^3\mathbf{8}_{eq}$ to $^5\mathbf{8}_{ax}$ (see Figure S10).[49]

Preparations of different spin isomers with the triflate and perchlorate ligands ($[(PyTACN)Fe(O)(OTf)]^+$ (**7**) and $[(PyTACN)Fe(O)(ClO_4)]^+$ (**10**)) were not successful. The IRPD spectra of the complexes with the perchlorate ligand were identical regardless of their preparation (i.e., transfer from solution or by nitrate cleavage). For the $[(PyTACN)Fe(O)(OTf)]^+$ complexes, the IRPD spectrum of the ions prepared in the gas phase by the "nitrate cleavage" differs from that of the ions generated from solution, but the differences are not due to the expected change of the spin isomer. The detected additional bands rather suggest presence of isobaric ions with an oxidized ligand. Most probably, the initially generated quintet state isomers formed upon the nitrate cleavage are very reactive and the iron(IV)−oxo moiety attacks the ligand (probably at one of

DOI: 10.1021/jacs.6b12291
J. Am. Chem. Soc. 2017, 139, 2757−2765

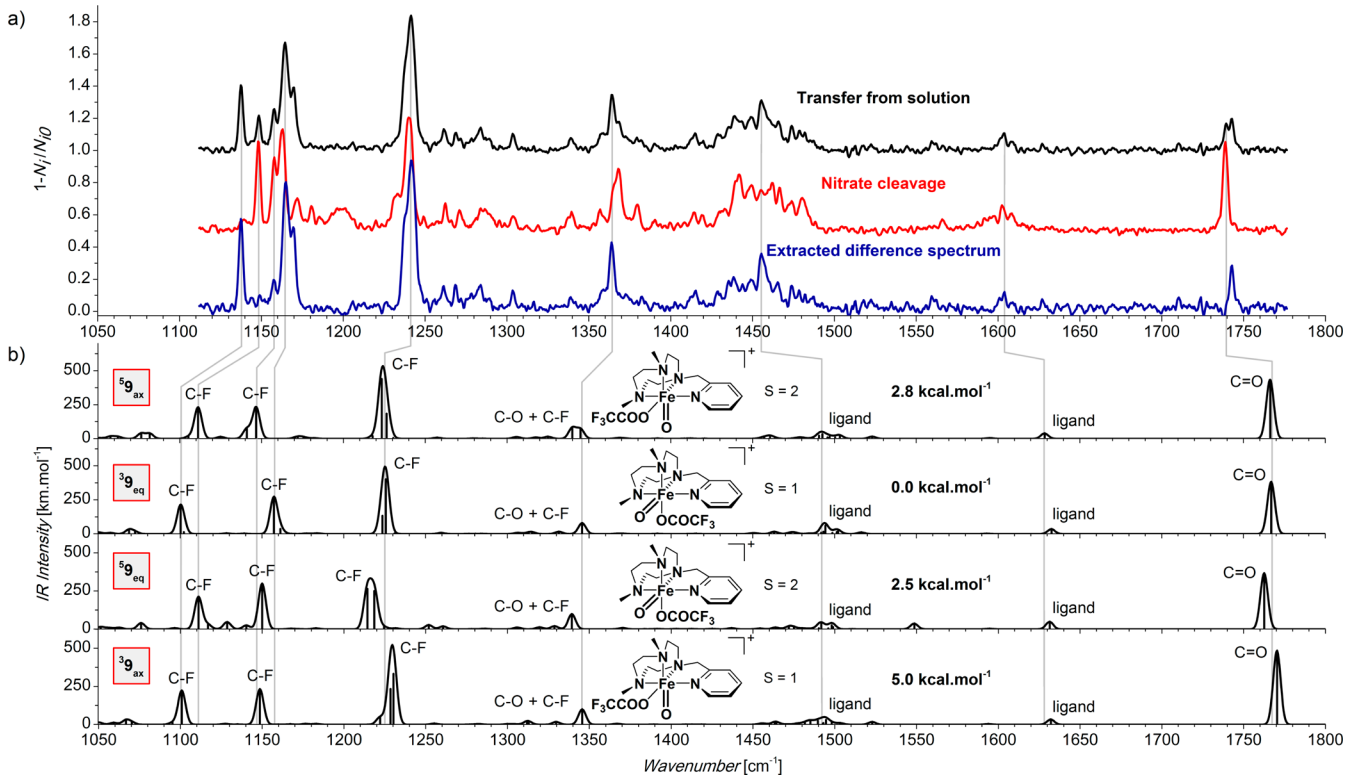

Figure 4. (a) IRPD spectra of the $[(PyTACN)Fe(O)(CF_3COO)]^+$ isomers generated by ligand exchange from the solution of $[(PyTACN)Fe(O)(CH_3CN)]^{2+}$ (the upper trace), generated in the gas phase from $[(PyTACN)Fe(NO_3)(CF_3COO)]^+$ by the nitrate cleavage (the middle trace), and the extracted difference spectrum (the lowest trace). (b) Theoretically predicted spectra of various isomers at the B3LYP-D3/BS1 level of theory scaled by 0.99. Energies are calculated at the CASPT2 level (see Table S3 for the absolute values) with DFT zero-point energy corrections.

Table 2. Reactivities of $[(L)Fe(O)(X)]^{2+/+}$ Complexes with 1,4-Cyclohexadiene-1,2,3,4,5,6-d_6 in the Gas Phase[a]

entry	L/X	from[a]	total reactivity[b]	branching [%] HAT/DAT/OAT	KIE
1	TMC/CH_3CN (**1**)	sol	360 ± 190	72:28:0[c]	2.5 ± 0.6
2	TMC/CF_3SO_3 (**2**)	sol	<3		
3	N4Py/− (**4**)	sol	10 ± 6	85:15:0[c,d]	5.7 ± 2.1
4	N4Py/CF_3SO_3 (**5**)	sol	5 ± 2	56:15:29	3.7 ± 0.4 (6.8)[e]
5	PyTACN/CH_3CN (**6**)	sol	900 ± 400	79:21:0[c]	3.8 ± 0.5
6	PyTACN/CF_3SO_3 (**7**)	sol	454 ± 11	56:16:28	3.5 ± 0.3
7	PyTACN/CF_3SO_3 (**7**)	frag	187 ± 46[f]	56:13:31	4.3 ± 0.2
8	PyTACN/NO_3 (**8**)	sol	100 ± 8	78:14:8	5.6 ± 0.1
9	PyTACN/NO_3 (**8**)	frag	195 ± 10	74:16:10	4.6 ± 0.3
10	PyTACN/CF_3COO (**9**)	sol	67 ± 13	76:14:9	5.4 ± 1.4
11	PyTACN/CF_3COO (**9**)	frag	238 ± 52	72:16:12	4.5 ± 0.2
12	PyTACN/ClO_4 (**10**)	sol	260	63:17:20	3.7
13	PyTACN/ClO_4 (**10**)	frag	261 ± 12	59:16:25	3.7 ± 0.3

[a]The $[(PyTACN)Fe(O)(X)]^+$ complexes were generated by oxidation in solution and transferred by ESI to the gas phase (denoted as sol) or by a fragmentation of their iron(III) nitrate precursors during the electrospray process (denoted as frag) [b]Total reactivity (sum of the rate constants for HAT, DAT, and OAT) is given relative to the reactivity of $[(PyTACN)Fe(O)(NO_3)]^+$ transferred from the solution, which was determined to be $(8.4 \pm 3.1) \times 10^{-12}$ cm^3 s^{-1} (ref 49) and is set as 100 here. [c]For dications, we observe a transfer of H^-/D^- instead of HAT and DAT (reactions 1 and 2 in the text). Note that for **1** and **6** the H^-/D^- transfer is associated with the elimination of acetonitrile. [d]We have observed also the electron transfer channel (7% with respect to the total reactivity). We assume that this channel is due to a reaction with an impurity. See the Supporting Information for details. [e]The measured kinetic isotope effect (KIE) is affected by a presence of an isobaric impurity (m/z 588) which undergoes a Coulomb explosion to ions with m/z 586 and m/z 589. After subtraction of this impurity, we obtain a KIE of 6.8. [f]Note that this number is hampered by the fact that we worked with a mixture of **7** with unreactive Fe^{II} complexes with an oxidized ligand.

the nitrogen atoms of the ligand, forming the corresponding amine *N*-oxide (cf. Figure S13).[53] The prediction of the theoretical spectra is not sufficiently accurate to allow us to unequivocally assign the spin states of **7** and **10** (Figures S13 and S14). Without an access to both spin states, we cannot judge the band shifts in the spectrum.

Reactivity of the Complexes. The access to the characterized iron(IV)−oxo complexes provides an opportunity to compare their unique reactivities. We have used 1,4-cyclohexadiene-1,2,3,4,5,6-d_6 (its preparation is described in ref 49) as a probe reactant because it enables us to compare hydrogen-atom transfer (HAT), deuterium-atom transfer

DOI: 10.1021/jacs.6b12291
J. Am. Chem. Soc. 2017, 139, 2757−2765

(DAT), and oxygen-atom transfer (OAT) in one step (Table 1 and Figures S19–S24).

First, we compared doubly charged iron(IV)–oxo complexes with different ligands (**1**, **4**, and **6**).[54,55] Gaseous reactions of dications with neutral molecules lead usually to the formation of two singly charged ions.[56] Here, we observe H^- and D^- transfers instead of HAT and DAT as predicted theoretically.[54,55] Formation of two singly charged ions from a dication-neutral couple is usually rather exothermic. Gaseous ions cannot dissipate the excess energy to solvent molecules. Instead, they undergo subsequent fragmentations. Here, we see a subsequent elimination of the acetonitrile molecule from complexes **1** and **6** (reactions 1 and 2; $n = 1$ for **1** and **6** and $n = 0$ for **4**). We do not see the OAT channel in the reactivity of dications. We note that the observed reactivity that suppresses formation of doubly charged products can be a sole property of gaseous complexes because of the lack of solvation that would stabilize the doubly charged products. Nevertheless, there might be some relevance to condensed phase reactions (see refs 57–59).

$$[(L)Fe(O)(CH_3CN)_n]^{2+} + C_6H_2D_6 \rightarrow [(L)Fe(OH)]^+ + nCH_3CN + C_6HD_6^+ \quad (1)$$

$$[(L)Fe(O)(CH_3CN)_n]^{2+} + C_6H_2D_6 \rightarrow [(L)Fe(OD)]^+ + nCH_3CN + C_6H_2D_5^+ \quad (2)$$

The total reactivities of the dicationic complexes can be ordered as **6** > **1** ≫ **4** (entries 5, 1, and 3 in Table 2). This result is not in agreement with previously observed reactivities of these ions in solution with weak C–H bonds, such as in 9,10-dihydroanthracene, that can be ordered according to ligands as PyTACN ≈ N4Py > TMC (Figure S18 in the Supporting Information). The differences can arise from a solvent effect or from the involvement of the present anions.

All complexes were generated from their triflate precursors; we have therefore compared the reactivities of the respective monocations **2**, **5**, and **7** bearing triflate as a ligand (entries 2, 4, and 6 in Table 2). The singly charged complexes follow the expected reaction channels: hydrogen-atom transfer, deuterium-atom transfer, and oxygen-atom transfer. Oxygen-atom transfer shows no KIE, indicating that the reaction corresponds to the epoxidation of the double bond (cf. Table S1 in the Supporting Information). Somewhat surprisingly, the total reactivities of monocations **5** (N4Py ligand) and **7** (PyTACN ligand) are on the same order of magnitude as those of the respective dications. On the other hand, the singly charged complex with the TMC ligand, **2**, is unreactive under the same conditions. This probably stems from the nature of the coordination of the anionic ligand. Triflate is *cis*-coordinated to the oxo group in complex **7**, which leads to about 50% drop in the total reactivity (cf. entries 5 and 6 in Table 2). Complex **5** contains triflate as a loosely bound counterion (the IRPD spectrum of complex **5** shows that triflate is not coordinated to iron; see Figure S8 in the Supporting Information). This loose binding leads also to about 50% reactivity drop (cf. entries 3 and 4 in Table 2). Finally, the TMC ligand allows coordination of triflate only in the *trans*-position with respect to the oxo group, which is probably the reason for the drastic attenuation of the observed total reactivity.

The formation of the triflate-coordinated complexes **2** can thus affect the overall reactivity of the TMC complexes by decreasing a number of the reactive species **1** in solution. The same process should not significantly influence the reactivity of the complexes with N4Py and PyTACN ligands. It can thus explain the observed reactivity trend in the condensed phase (Figure S18 in the Supporting Information).

We have further compared relative reactivities in dependence of the anionic ligand and the spin state for complexes **7**–**10** (entries 6–13 in Table 2). The reactivities decrease in the following order: **7** > **10** > ^{5}**9**$_{ax}$ > ^{5}**8**$_{ax}$ > ^{3}**8**$_{eq}$ > ^{3}**9**$_{eq}$ (we did not assign the spin isomers of **7** and **10**; see above). The $S = 2$ spin isomers of **8** and **9** are more reactive than their $S = 1$ analogues. With the increasing reactivity, the kinetic isotope effect for HAT versus DAT clearly decreases. Further, the relative abundance of the OAT channel correlates with the total reactivity. Its ratio increases with the increasing total reactivity. This channel is much more sensitive to the nature of the anion ligand than to the spin state of the complex (cf. Figure 5).[60]

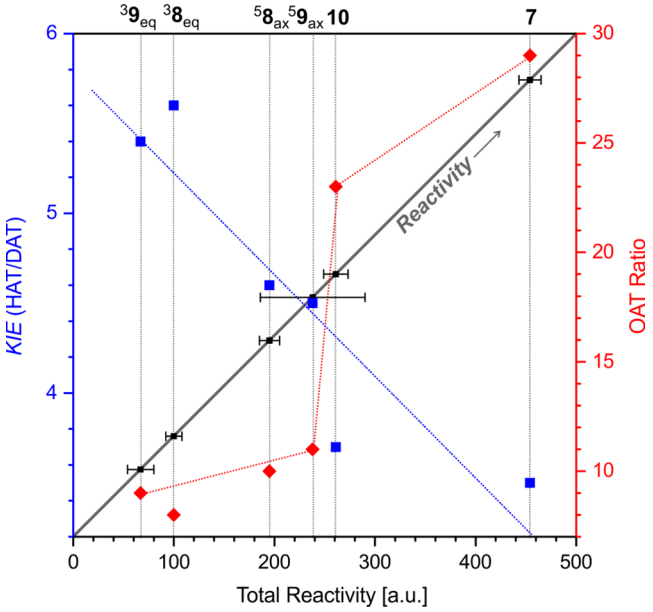

Figure 5. Comparison of gas-phase reactivity of complexes **7**–**10** with 1,4-cyclohexadiene-1,2,3,4,5,6-d_6 (see also Table 2). The error bars denote the standard deviation of the total reactivities. The dotted lines serve as a guide for the eyes.

We have also measured reactivities of the gas-phase-generated **7** and **10**. As mentioned above, for complex **10**, this method leads to the ions with identical spectral characteristics as the ions transferred from the oxidized solution. In agreement, the reactivities of the ions generated in both ways are identical. We can easily rationalize this result based on the quantum chemical calculations. The perchlorate ligand preferentially occupies the axial position of the complex in both spin states (i.e., the oxo group is always in the equatorial position; ^{3}**10**$_{eq}$ and ^{5}**10**$_{eq}$ are the preferred spin isomers). The CASPT2 calculations predict that the quintet state isomer ^{5}**10**$_{eq}$ is preferred in the gas phase. Regardless, whether we transfer or generate the $S = 1$ or $S = 2$ state during the electrospray ionization, we expect that, due to the fast spin isomerization at the iron center, we always detect reactivity of the preferred spin isomer (i.e., ^{5}**10**$_{eq}$).

For the triflate-bound complex **7**, the reactivity of the ions generated by the gas-phase fragmentation significantly drops. This is also in accordance with our spectroscopic experiments that showed that these ions are contaminated by the isomers with an oxidized ligand. Triflate, similarly to perchlorate, always

DOI: 10.1021/jacs.6b12291
J. Am. Chem. Soc. 2017, 139, 2757–2765

occupies the axial position. We have therefore the same situation as for **10**. We generate a mixture of $^{3}\mathbf{7}_{eq}$ and $^{5}\mathbf{7}_{eq}$ that rapidly spin isomerizes to the preferred spin state in the gas phase (the CASPT2 calculations predict both of the spin isomers to be essentially isoenergetic). We rationalize the drop in the reactivity for the complexes generated by the nitrate cleavage by the large reactivity of the triflate complexes (cf. Table 2). The gas-phase-generated ions are initially formed with a large internal energy excess. Under the same conditions, we are able to thermalize the less reactive ions (**8**, **9**, and **10**) by collisional cooling with the sheath gas (N_2) before they undergo the internal oxidation. For complex **7**, the internal oxidation proceeds probably much faster, and therefore, a substantial amount of ions isomerize before we are able to cool them to ambient temperature.

CONCLUSIONS

We present helium tagging infrared spectroscopy as a unique tool to characterize iron(IV)−oxo complexes. We can unequivocally determine the Fe=O vibration as well as other spectral features in mass-selected reactive complexes. We have shown the comparison of gas-phase features with known data from solution. We show that solvation influences the Fe=O vibration. In acetonitrile, an average red shift of 9 cm^{-1} was observed. In addition, we have compared reactivities of the characterized gaseous complexes toward 1,4-cyclohexadiene. We show that the nature of the anion coordinated as a ligand as well as the polydentate ligand itself has a substantial effect on the reactivity. Comparison of the relative reactivities suggests that it might be necessary to include the counterion effect when comparing the reactivities of the complexes in solution. We further show that the anionic ligands influence the relative stabilities of the $S = 1$ and $S = 2$ states and play a role in oxygen-transfer reactions toward C=C bonds. For complex **8** that we were able to generate as two spin isomers ($^{3}\mathbf{8}_{eq}$ and $^{5}\mathbf{8}_{ax}$), we established that the Fe=O vibration differs only by 1 cm^{-1}. We demonstrate that the $S = 1$ and $S = 2$ states can be distinguished based on the vibrations of the anionic ligands.

ASSOCIATED CONTENT

Supporting Information

The Supporting Information is available free of charge on the ACS Publications website at DOI: 10.1021/jacs.6b12291.

Further experimental details, all experimental and calculated spectra, gas-phase reactivities, theoretical results, and complete ref 23 (PDF)

Calculated structures (XYZ)

AUTHOR INFORMATION

Corresponding Authors

*martin.srnec@jh-inst.cas.cz

*miquel.costas@udg.edu

*roithova@natur.cuni.cz

ORCID

Martin Srnec: 0000-0001-5118-141X

Miquel Costas: 0000-0001-6326-8299

Jana Roithová: 0000-0001-5144-0688

Notes

The authors declare no competing financial interest.

ACKNOWLEDGMENTS

Computational resources were provided by the MetaCentrum under the program LM2010005 and the CERIT-SC under the program Centre CERIT Scientific Cloud, part of the Operational Program Research and Development for Innovations, Reg. No. CZ.1.05/3.2.00/08.0144. The project was supported by the Czech Science Foundation (14-20077S and 15-10279Y), European Research Council (ERC CoG No. 682275), and the COST action ECOSTBio. M.S. is also grateful to to the Czech Academy of Sciences for the Purkyně fellowship.

REFERENCES

(1) (a) Abu-Omar, M. M.; Loaiza, A.; Hontzeas, N. *Chem. Rev.* **2005**, *105*, 2227−2252. (b) Stone, K. L.; Borovik, A. S. *Curr. Opin. Chem. Biol.* **2009**, *13*, 114−118. (c) Solomon, E. I.; Light, K. M.; Liu, L. V.; Srnec, M.; Wong, S. D. *Acc. Chem. Res.* **2013**, *46*, 2725−2739. (d) *Iron-Containing Enzymes: Versatile Catalysts of Hydroxylation Reactions in Nature*; de Visser, S. P., Kumar, D., Eds.; RSC Publishing: Cambridge, U.K., 2011. (e) Company, A.; Lloret-Fillol, J.; Costas, M. Small Molecule Models for Nonporphyrinic Iron and Manganese Oxygenases. In *Comprehensive Inorganic Chemistry II*; Reedijk, J., Poeppelmeier, K., Eds.; Elsevier: Oxford, 2013; Vol. 3.

(2) (a) Price, J. C.; Barr, E. W.; Tirupati, B.; Bollinger, J. M., Jr.; Krebs, C. *Biochemistry* **2003**, *42*, 7497. (b) Bollinger, J. M., Jr.; Krebs, C. *J. Inorg. Biochem.* **2006**, *100*, 586. (c) Krebs, C.; Galonić Fujimori, D.; Walsh, C. T.; Bollinger, J. M., Jr. *Acc. Chem. Res.* **2007**, *40*, 484.

(3) Rohde, J.-H.; In, M.-H.; Lim, W. W.; Brennessel, M. R.; Bukowski, A.; Stubna, E.; Münck, W.; Nam, J.; Que, L. *Science* **2003**, *299*, 1037−1039.

(4) (a) Nam, W. *Acc. Chem. Res.* **2007**, *40*, 522−531. (b) Nam, W.; Lee, Y.-M.; Fukuzumi, S. *Acc. Chem. Res.* **2014**, *47*, 1146−1154. (c) Ray, K.; Pfaff, F. F.; Wang, B.; Nam, W. *J. Am. Chem. Soc.* **2014**, *136*, 13942−13958.

(5) (a) McDonald, A. R.; Que, L., Jr. *Coord. Chem. Rev.* **2013**, *257*, 414−428. (b) Puri, M.; Que, L., Jr. *Acc. Chem. Res.* **2015**, *48*, 2443−2452.

(6) Sastri, C. V.; Park, M. J.; Ohta, T.; Jackson, T. A.; Stubna, A.; Seo, M. S.; Lee, J.; Kim, J.; Kitagawa, T.; Munck, E.; Que, L., Jr.; Nam, W. *J. Am. Chem. Soc.* **2005**, *127*, 12494−12495.

(7) (a) Klein, J. E. M. N.; Que, L., Jr. Biomimetic High-Valent Mononuclear Nonheme Iron-Oxo Chemistry. In *Encyclopedia of Inorganic and Bioinorganic Chemistry*; Scott, R. A., Ed.; John Wiley: Chichester, U.K., 2016. (b) Hohenberger, J.; Ray, K.; Meyer, K. *Nat. Commun.* **2012**, *3*, 720.

(8) Wang, D.; Ray, K.; Collins, M. J.; Farquhar, E. R.; Frisch, J. R.; Gómez, L.; Jackson, T. A.; Kerscher, M.; Waleska, A.; Comba, P.; Costas, M.; Que, L., Jr. *Chem. Sci.* **2013**, *4*, 282−291.

(9) (a) Rohde, J.-U.; Stubna, A.; Bominaar, E. L.; Munck, E.; Nam, W.; Que, L., Jr. *Inorg. Chem.* **2006**, *45*, 6435−6445. (b) Planas, O.; Clemancey, M.; Latour, J.-M.; Company, A.; Costas, M. *Chem. Commun.* **2014**, *50*, 10887−10890.

(10) Ye, S.; Kupper, C.; Meyer, S.; Andris, E.; Navratil, R.; Krahe, O.; Mondal, B.; Atanasov, M.; Bill, E.; Roithova, J.; Meyer, F.; Neese, F. *J. Am. Chem. Soc.* **2016**, *138*, 14312−14325.

(11) McLuckey, S. A.; Wells, J. M. *Chem. Rev.* **2001**, *101*, 571−606.

(12) (a) To, W.-P.; Wai-Shan Chow, T.; Tse, C.-W.; Guan, X.; Huang, J.-S.; Che, C.-M. *Chem. Sci.* **2015**, *6*, 5891. (b) Prat, I.; Mathieson, J. S.; Güell, M.; Ribas, X.; Luis, J. M.; Cronin, L.; Costas, M. *Nat. Chem.* **2011**, *3*, 788. (c) Hitomi, Y.; Arakawa, K.; Funabiki, T.; Kodera, M. *Angew. Chem., Int. Ed.* **2012**, *51*, 3448−3452.

(13) Theron, R.; Wu, Y.; Yunker, L. P. E.; Hesketh, A. V.; Pernik, I.; Weller, A. S.; McIndoe, J. S. *ACS Catal.* **2016**, *6*, 6911−6917.

(14) (a) Douberly, G. E.; Walters, R. S.; Cui, J.; Jordan, K. D.; Duncan, M. A. *J. Phys. Chem. A* **2010**, *114*, 4570−4579. (b) Rizzo, T. R.; Boyarkin, O. V. *Topics in Current Chemistry*; Springer International Publishing: Berlin, 2014; Vol. 364, pp 43−97. (c) Heine, N.; Fagiani, M. R.; Rossi, M.; Wende, T.; Berden, G.; Blum, V.; Asmis, K. R. *J. Am. Chem. Soc.*

DOI: 10.1021/jacs.6b12291
J. Am. Chem. Soc. 2017, 139, 2757−2765

2013, *135*, 8266−8273. (d) Wolk, A. B.; Leavitt, C. M.; Garand, E.; Johnson, M. A. *Acc. Chem. Res.* **2014**, *47*, 202−210.
(15) (a) Roithová, J.; Gray, A.; Andris, E.; Jašík, J.; Gerlich, D. *Acc. Chem. Res.* **2016**, *49*, 223−230. (b) Jašík, J.; Gerlich, D.; Roithová, J. *J. Am. Chem. Soc.* **2014**, *136*, 2960−2962. (c) Jašík, J.; Navrátil, R.; Němec, I.; Roithová, J. *J. Phys. Chem. A* **2015**, *119*, 12648−12655. (d) Schulz, J.; Jašík, J.; Gray, A.; Roithová, J. *Chem. - Eur. J.* **2016**, *22*, 9827−9834.
(16) (a) Seo, M. S.; In, J.-H.; Kim, S. O.; Oh, N. Y.; Hong, J.; Kim, J.; Que, L., Jr.; Nam, W. *Angew. Chem., Int. Ed.* **2004**, *43*, 2417−2420. (b) Puri, M.; Company, A.; Sabenya, G.; Costas, M.; Que, L., Jr. *Inorg. Chem.* **2016**, *55*, 5818−5827.
(17) (a) Ducháčková, L.; Roithová, J. *Chem. - Eur. J.* **2009**, *15*, 13399. (b) Jašíková, L.; Roithová, J. *Organometallics* **2012**, *31*, 1935.
(18) Kaizer, J.; Klinker, E. J.; Oh, N. Y.; Rohde, J.-U.; Song, W. J.; Stubna, A.; Kim, J.; Münck, E.; Nam, W.; Que, L., Jr. *J. Am. Chem. Soc.* **2004**, *126*, 472−473.
(19) Company, A.; Prat, I.; Frisch, J. R.; Mas-Ballesté, R.; Güell, M.; Juhász, G.; Ribas, X.; Münck, E.; Luis, J. M.; Que, L., Jr.; Costas, M. *Chem. - Eur. J.* **2011**, *17*, 1622−1634.
(20) (a) Jackson, T. A.; Rohde, J.-U.; Seo, M. S.; Sastri, C. V.; DeHont, R.; Stubna, A.; Ohta, T.; Kitagawa, T.; Münck, E.; Nam, W.; Que, L., Jr *J. Am. Chem. Soc.* **2008**, *130*, 12394−12407. (b) Sastri, C. V.; Lee, J.; Oh, K.; Lee, Y. J.; Lee, J.; Jackson, T. A.; Ray, K.; Hirao, H.; Shin, W.; Halfen, J. A.; Kim, J.; Que, L.; Shaik, S.; Nam, W. *Proc. Natl. Acad. Sci. U. S. A.* **2007**, *104*, 19181−19186.
(21) Ervin, K. M.; Armentrout, P. B. *J. Chem. Phys.* **1985**, *83*, 166−189.
(22) Jašík, J.; Žabka, J.; Roithová, J.; Gerlich, D. *Int. J. Mass Spectrom.* **2013**, *354*−*355*, 204−210.
(23) Frisch, M. J.; et al. *Gaussian 09*, revision D.01; Gaussian, Inc.: Wallingford, CT, 2013.
(24) (a) Becke, A. D. *J. Chem. Phys.* **1993**, *98*, 5648−5652. (b) Lee, C.; Yang, W.; Parr, R. G. *Phys. Rev. B: Condens. Matter Mater. Phys.* **1988**, *37*, 785. (c) Miehlich, B.; Savin, A.; Stoll, H.; Preuss, H. *Chem. Phys. Lett.* **1989**, *157*, 200−206. (d) Stephens, P. J.; Devlin, F. J.; Chabalowski, C. F.; Frisch, M. J. *J. Phys. Chem.* **1994**, *98*, 11623−11627.
(25) (a) Becke, A. D. *Phys. Rev. A: At., Mol., Opt. Phys.* **1988**, *38*, 3098. (b) Perdew, J. P. *Phys. Rev. B: Condens. Matter Mater. Phys.* **1986**, *33*, 8822.
(26) Hamprecht, F. A.; Cohen, A.; Tozer, D. J.; Handy, N. C. *J. Chem. Phys.* **1998**, *109*, 6264−6271.
(27) Wilson, P. J.; Bradley, T. J.; Tozer, D. J. *J. Chem. Phys.* **2001**, *115*, 9233−9242.
(28) Grimme, S.; Ehrlich, S.; Goerigk, L. *J. Comput. Chem.* **2011**, *32*, 1456−1465.
(29) Vosko, S. H.; Wilk, L.; Nusair, M. *Can. J. Phys.* **1980**, *58*, 1200−1211.
(30) (a) Handy, N. C.; Cohen, A. J. *Mol. Phys.* **2001**, *99*, 403−12. (b) Hoe, W.-M.; Cohen, A.; Handy, N. C. *Chem. Phys. Lett.* **2001**, *341*, 319−28.
(31) (a) Perdew, J. P.; Burke, K.; Ernzerhof, M. *Phys. Rev. Lett.* **1996**, *77*, 3865−68. (b) Perdew, J. P.; Burke, K.; Ernzerhof, M. *Phys. Rev. Lett.* **1997**, *78*, 1396.
(32) Zhao, Y.; Truhlar, D. G. *Theor. Chem. Acc.* **2008**, *120*, 215−241.
(33) Zhao, Y.; Truhlar, D. G. *J. Chem. Phys.* **2006**, *125*, 194101.
(34) Yanai, T.; Tew, D.; Handy, N. *Chem. Phys. Lett.* **2004**, *393*, 51−57.
(35) (a) Perdew, J. P. In *Electronic Structure of Solids '91*; Ziesche, P., Eschig, H., Eds.; Akademie Verlag: Berlin, 1991; p 11. (b) Adamo, C.; Barone, V. *J. Chem. Phys.* **1998**, *108*, 664−675.
(36) Adamo, C.; Barone, V. *J. Chem. Phys.* **1999**, *110*, 6158−6169.
(37) Tao, J. M.; Perdew, J. P.; Staroverov, V. N.; Scuseria, G. E. *Phys. Rev. Lett.* **2003**, *91*, 146401.
(38) Staroverov, V. N.; Scuseria, G. E.; Tao, J.; Perdew, J. P. *J. Chem. Phys.* **2003**, *119*, 12129.
(39) Grimme, S.; Ehrlich, S.; Goerigk, L. *J. Comput. Chem.* **2011**, *32*, 1456−1465.
(40) (a) Jensen, F. *J. Chem. Phys.* **2001**, *115*, 9113. (b) Jensen, F. *J. Chem. Phys.* **2002**, *116*, 7372. (c) Jensen, F.; Helgaker, T. *J. Chem. Phys.* **2004**, *121*, 3463.
(41) Boese, A. D.; Martin, J. M. L. *J. Mol. Struct.* **2006**, *780*−*781*, 310−316.
(42) (a) Roos, B. O.; Taylor, P. R.; Siegbahn, P. E. M. *Chem. Phys.* **1980**, *48*, 157−173. (b) Siegbahn, P. E. M.; Almlöf, J.; Heiberg, A.; Roos, B. O. *J. Chem. Phys.* **1981**, *74*, 2384−2396.
(43) (a) Andersson, K.; Malmqvist, P.-Å.; Roos, B. O.; Sadlej, A. J.; Wolinski, K. *J. Phys. Chem.* **1990**, *94*, 5483−5488. (b) Andersson, K.; Malmqvist, P.-Å.; Roos, B. O. *J. Chem. Phys.* **1992**, *96*, 1218−1226. (c) Andersson, K. *Theor. Chim. Acta* **1995**, *91*, 31−46. (d) Finley, J.; Malmqvist, P.-Å.; Roos, B. O.; Serrano-Andrés, L. *Chem. Phys. Lett.* **1998**, *288*, 299−306.
(44) Aquilante, F.; Pedersen, T. B.; Lindh, R.; Roos, B. O.; Sánchez de Merás, A.; Koch, H. *J. Chem. Phys.* **2008**, *129*, 024113.
(45) (a) Douglas, M.; Kroll, N. M. *Ann. Phys. (Amsterdam, Neth.)* **1974**, *82*, 89−155. (b) Hess, B. A. *Phys. Rev. A: At., Mol., Opt. Phys.* **1986**, *33*, 3742−3748. (c) Jansen, G.; Hess, B. A. *Phys. Rev. A: At., Mol., Opt. Phys.* **1989**, *39*, 6016−6017.
(46) Aquilante, F.; Malmqvist, P.-Å.; Pedersen, T. B.; Ghosh, A.; Roos, B. O. *J. Chem. Theory Comput.* **2008**, *4*, 694−702.
(47) (a) Roos, B. O.; Andersson, K. *Chem. Phys. Lett.* **1995**, *245*, 215−243. (b) Forsberg, N.; Malmqvist, P.-Å. *Chem. Phys. Lett.* **1997**, *274*, 196−204.
(48) Prakash, J.; Rohde, G. T.; Meier, K. K.; Münck, E.; Que, L., Jr. *Inorg. Chem.* **2015**, *54*, 11055−11057.
(49) Andris, E.; Jašík, J.; Gómez, L.; Costas, M.; Roithová, J. *Angew. Chem., Int. Ed.* **2016**, *55*, 3637−3641.
(50) (a) Duffy, E. M.; Marsh, B. M.; Voss, J. M.; Garand, E. *Angew. Chem., Int. Ed.* **2016**, *55*, 4079−4082. (b) Škríba, A.; Jašík, J.; Andris, E.; Roithová, J. *Organometallics* **2016**, *35*, 990−994. (c) Fridgen, T. D. *Mass Spectrom. Rev.* **2009**, *28*, 586−607. (d) Nosenko, Y.; Menges, F.; Riehn, C.; Niedner-Schatteburg, G. *Phys. Chem. Chem. Phys.* **2013**, *15*, 8171−8178. (e) Ingram, J.; Wolk, A. B.; Flender, C.; Zhang, J.; Johnson, C. J.; Hintermair, U.; Crabtree, R. H.; Johnson, M. A.; Zare, R. N. *Inorg. Chem.* **2014**, *53*, 423−433. (f) Jašíková, L.; Hanikýřová, E.; Schröder, D.; Roithová, J. *J. Mass Spectrom.* **2012**, *47*, 460−465. (g) Jašíková, L.; Hanikýřová, E.; Škríba, A.; Jašík, J.; Roithová, J. *J. Org. Chem.* **2012**, *77*, 2829−2936. (h) Roithová, J.; Milko, P. *J. Am. Chem. Soc.* **2010**, *132*, 281−288. (i) Chiavarino, B.; Crestoni, M. E.; Fornarini, S.; Lanucara, F.; Lemaire, J.; Maitre, P. *Angew. Chem., Int. Ed.* **2007**, *46*, 1995−1998.
(51) It was shown that solvation affects the entropy of solvated molecules which is not well treated at the DFT level of theory. This might affect theoretical predictions of IR spectra. While this should not concern our spectra measured in the gas phase at 3 K, it might be important for prediction of IR spectra at higher temperatures and in the condensed phase. See also: Cantu Reinhard, F. G.; Faponle, A. S.; de Visser, S. P. *J. Phys. Chem. A* **2016**, *120*, 9805−9814.
(52) Schröder, D.; Roithová, J.; Schwarz, H. *Int. J. Mass Spectrom.* **2006**, *254*, 197−201.
(53) Nielsen, A.; Larsen, F. B.; Bond, A. D.; McKenzie, C. J. *Angew. Chem., Int. Ed.* **2006**, *45*, 1602−1606.
(54) DFT calculations of the potential energy pathway for the reaction between **1** or **1**·CF_3COO^- and C_6H_8 can be found at: Hirao, H.; Que, L., Jr.; Nam, W.; Shaik, S. *Chem. - Eur. J.* **2008**, *14*, 1740.
(55) DFT calculations of the potential energy pathway for the reaction between **4** or **4**·$(ClO_4)_2^-$ and C_6H_8 can be found at: Janardanan, D.; Usharani, D.; Chen, H.; Shaik, S. *J. Phys. Chem. Lett.* **2011**, *2*, 2610−2617.
(56) Roithová, J.; Schröder, D. *Phys. Chem. Chem. Phys.* **2007**, *9*, 2341−2349.
(57) Kim, S.; Cho, K.-B.; Lee, Y.-M.; Chen, J.; Fukuzumi, S.; Nam, W. *J. Am. Chem. Soc.* **2016**, *138*, 10654−10663.
(58) Oloo, W. N.; Feng, Y.; Iyer, S.; Parmelee, S.; Xue, G.; Que, L., Jr. *New J. Chem.* **2013**, *37*, 3411−3415.
(59) Kwon, Y. H.; Mai, B. K.; Lee, Y.-M.; Dhuri, S. N.; Mandal, D.; Cho, K.-B.; Kim, Y.; Shaik, S.; Nam, W. *J. Phys. Chem. Lett.* **2015**, *6*, 1472−1476.
(60) Theoretical studies involving the anion effect: (a) Hirao, H.; Kumar, D.; Que, L., Jr.; Shaik, S. *J. Am. Chem. Soc.* **2006**, *128*, 8590−

DOI: 10.1021/jacs.6b12291
J. Am. Chem. Soc. 2017, 139, 2757−2765

8606. (b) Johansson, A. J.; Blomberg, M. R. A.; Siegbahn, P. E. M. *J. Phys. Chem. C* **2007**, *111*, 12397−12406.

DOI: 10.1021/jacs.6b12291
J. Am. Chem. Soc. 2017, 139, 2757−2765